Signal-to-noise performance of a short-wave infrared nanoinjection imager

Omer Gokalp Memis, John Kohoutek, Wei Wu, Ryan M. Gelfand, and Hooman Mohseni*

Department of Electrical Engineering and Computer Science, Northwestern University, Evanston, Illinois 60208, USA

**Corresponding author: hmohseni@northwestern.edu*

Received April 23, 2010; revised June 22, 2010; accepted July 13, 2010; posted July 20, 2010 (Doc. ID 127345); published August 6, 2010

We report on the signal-to-noise performance of a nanoinjection imager, which is based on a short-wave IR InGaAs/GaAsSb/InP detector with an internal avalanche-free amplification mechanism. Test pixels in the imager show responsivity values reaching 250 A/W at 1550 nm, −75 °C, and 1.5 V due to an internal charge amplification mechanism in the detector. In the imager, the measured imager noise was 28 electrons (e^-) rms at a frame rate of 1950 frames/s. Additionally, compared to a high-end short-wave IR imager, the nanoinjection camera shows 2 orders of magnitude improved signal-to-noise ratio at thermoelectric cooling temperatures primarily due to the small excess noise at high amplification. © 2010 Optical Society of America

OCIS codes: 110.3080, 040.3780.

Highly sensitive short-wave IR (SWIR) imagers are essential components in many applications both in existing fields and also in emerging state-of-the-art applications. In military and homeland security applications, short-wave IR offers significant illumination at night, also called the night glow or night spectral radiance [1,2]. With the aid of night glow, short-wave IR imagers can offer much higher signal-to-noise levels compared to other spectra at night. SWIR spectra can be used in nondestructive materials evaluation [3] and explosives detection [4] for commercial and homeland security purposes. For rapidly emerging telecommunication applications, such as quantum key distribution [5] and quantum computing [6,7], high sensitivity is not only needed in individual IR detectors but also in arrays of detectors, as it has been shown that arrays can speed up applications like parallel quantum computing tremendously [8]. In medicine, imaging tools, such as optical coherence tomography, would benefit from SWIR imagers: As the short-wave IR light offers significant penetration depth through tissues, such as skin [9], the noninvasive screening depth for these instruments would increase.

Here, we present our first imager results showing the potential of nanoinjection technology. It can provide high-fidelity internal amplification with small pixel sizes and a large number of pixels, which is currently a difficult task with mainstream technologies primarily due to noise considerations. The signal-to-noise ratio (SNR) of a photodetection system after the first amplifier can be expressed [10] as $\mathrm{SNR}_{\mathrm{total}} = S^2/(N^2_{\mathrm{detector}} + N^2_{\mathrm{amplifier}}/G^2_{\mathrm{detector}})$, where S is the signal at the input, N is the noise, and G is the amplification of the detector/pixel. This would mean that the noise contribution of the detector is unavoidable, but the contribution from the amplifier can be suppressed in the presence of gain in the detector stage.

The mainstream detector systems for short-wave spectra are the PIN detectors and avalanche photodetectors (APDs). The PIN detectors are low-current devices without internal amplification. To form imagers, they are coupled with electrical low-noise amplifiers called the readout integrated circuits (ROIC) [11]. However, even the lowest noise ROICs [12] have trouble retaining the signal-to-noise required with low-energy signals due to the lack of internal amplification in PIN detectors. The only mainstream solid-state photodetector platform that can provide linear-mode internal amplification is an avalanche APD. However, APDs require a high electric field, which can lead to edge breakdown, and need large guard rings to prevent this phenomenon [13]. The guard rings increase the pixel pitch and reduce the fill factor, which in turn lead to larger imager chips. Larger imager chips require larger and heavier optics, as the size and weight of the optics scale with the third power of pixel pitch [14]. Furthermore, the APD pixels need to be spaced apart to prevent cross talk due to generation-recombination and reemission of carriers [15]. Hence, realization of high-resolution imagers with high internal gain and low noise has remained a challenging task.

In our previous studies, we have reported the performance of individual nanoinjection detectors [16]. The nanoinjection detectors were able to provide internal amplification resulting in more than 10,000 injected electrons per absorbed photon at room temperature and bias voltages less than 1 V. The excess noise figure of the detectors were measured to be less than 1 at amplification values as high as 4000 [17], indicating strong noise suppression due to a feedback-stabilized internal amplification mechanism.

Because of these factors, we targeted at an imager based on the nanoinjection mechanism, which would offer improved sensitivity in smaller pixel sizes and complementary metal-oxide-semiconductor (CMOS) compatibility due to the low voltage requirements. We have fabricated a 320-by-240 pixel nanoinjection imager with 30 μm pitch using an off-the-shelf CMOS ROIC with 575–870 e^- rms noise, ISC9705 from Indigo (Fig. 1). Measuring the test pixels on the imager, we were able to characterize the current-voltage and responsivity performance of the imager at −75 °C, which showed 250 A/W responsivity at 1.5 V (Fig. 2). The measured FWHM diameter of the test pixel response is 30 μm, and the fill factor is 78%.

 © 2010 Optical Society of America

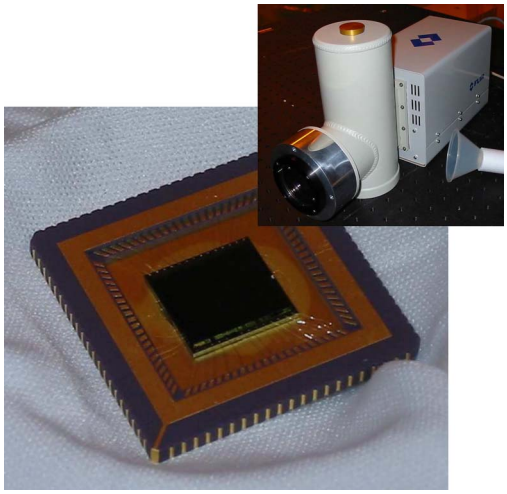

Fig. 1. (Color online) Photos of the imager chip and the camera kit are shown.

For imaging comparisons, a short-wave IR camera, AlphaNIR, from one of the largest producers of commercial IR imagers (FLIR) was used. AlphaNIR is a low dark-current InGaAs PIN-based focal plane array integrated with a high-performance, low-noise (50 e^- rms) ROIC, ISC9809 from Indigo [18]. The camera has the same pixel size and resolution as the nanoinjection imager and is internally TE-cooled to −7 °C. The nanoinjection imager was placed in an evaluation kit from Indigo, and was cooled to −7 °C or −75 °C. The integration time was set to 0.5 ms and $f/1.8$ lenses were used for both cameras. The dynamic range of both cameras was equalized by disabling the auto gain and contrast in both cameras while they were imaging the same scene (Fig. 3) (Media 1).

Besides the visual comparison of the cameras in a low-light-level scene, we measured the SNR histograms of the two cameras, as well as the absolute SNR of our camera. First, the images of a calibrated, uniform, and adjustable light source were acquired with both cameras for comparison. The signal was calculated by subtracting the dark scene from the illuminated scene, and the standard deviation of each pixel was calculated from its time evolution. The ratio of the signal squared to standard deviation squared yielded the SNR for each pixel. At −7 °C, the measured SNR of a nanoinjection imager was ∼11% better (∼7.1) compared to the commercial SWIR camera AlphaNIR (∼6.3). Under further cooling, the SWIR PIN-based imagers, including AlphaNIR, are limited by ROIC noise levels, which are almost temperature independent,

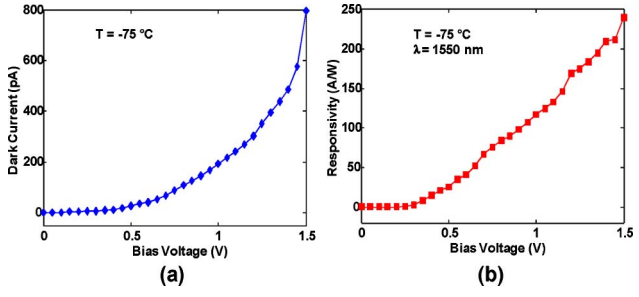

Fig. 2. (Color online) (a) Dark current and (b) responsivity of a test pixel of the nanoinjection imager are plotted at $T = -75$ °C.

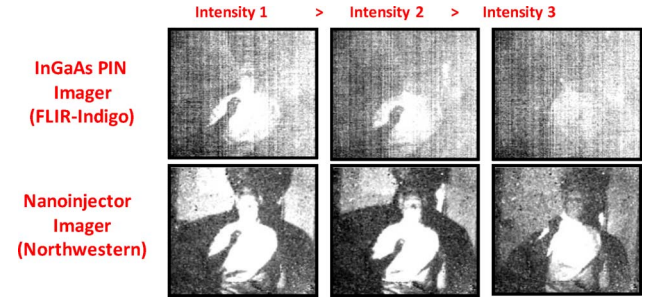

Fig. 3. (Color online) Comparison images of a commercial InGaAs SWIR imager and nanoinjection imager are shown (Media 1). The top row contains images from a commercial PIN-based SWIR imager acquired at different illuminations. The bottom row shows the images acquired from the same scenes at the same time using our nanoinjection imager.

as such conventional PIN imagers do not offer any significant improvement in SNR by cooling. However, the nanoinjection imagers show significant improvement at lower temperatures, and SNR of the nanoinjection camera at −75 °C was 2 orders of magnitude higher than the commercial SWIR camera (1656 versus 17.1), as shown in Fig. 4. Our nanoinjection imagers amplify the signal with a high fidelity before it reaches the readout electronics; hence, the performance was not limited by the electronic noise of the ROIC.

Second, a National Institute of Standards and Technology calibrated laser at 1.55 μm was focused onto the nanoinjection camera and images were acquired. The measured data were fitted to the following [19,20] to obtain excess noise and overall pixel noise:

$$\mathrm{SNR} = \frac{\Phi t_{\mathrm{int}} G^2}{G^2 F + \frac{\sigma}{\Phi t_{\mathrm{int}}}} = \frac{N^2}{FN + \frac{\sigma}{G^2}} = \frac{N^2}{FN + \sigma'_{\mathrm{overall}}},$$

$$N = \Phi t_{\mathrm{int}} = \frac{P_{\mathrm{opt}} t_{\mathrm{int}}}{E_{\mathrm{ph}}},$$

where Φ is photon flux/second, t_{int} is the integration time, G is the detector internal amplification, F is the excess noise factor, σ is the noise, N is the number of photons, $\sigma'_{\mathrm{overall}}$ is the overall input noise of the system, P_{opt} is the calibrated optical power, and E_{ph} is the photon energy. In this equation, the quantum efficiency is taken as 1, which would yield an upper bound on the noise amplitude and excess noise factor. At an integration time of

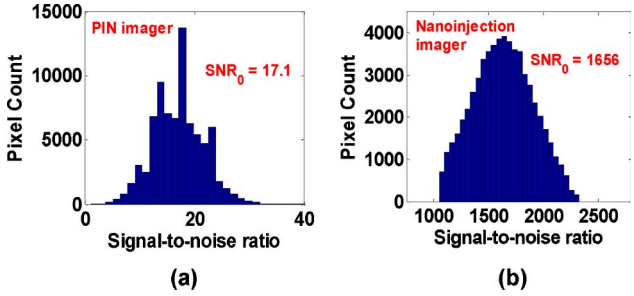

Fig. 4. (Color online) Comparison of the SNR histogram of the (a) commercial camera versus the histogram of our (b) nanoinjection imager indicates that the SNR of our imager (1656) is 2 orders of magnitude improvement over the commercial IR camera (17.1).

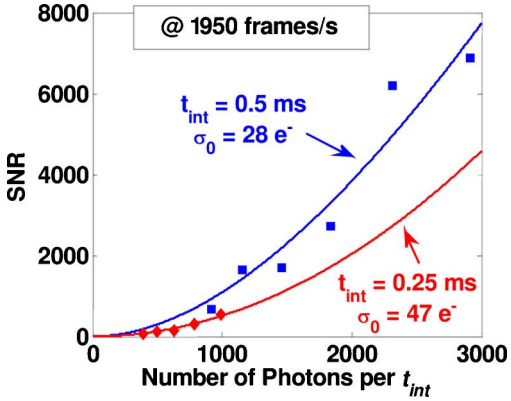

Fig. 5. (Color online) SNR of the nanoinjection imager versus number of photons, gathered using images acquired at different photon fluxes at a frame rate of 1950 frames/s is plotted. The analysis of the data reveals that the readout noise is 28 e^- at 0.5 ms integration time and 47 e^- at 0.25 ms.

0.5 ms and a frame rate of 1950 frames/s, the SNR analysis (Fig. 5) revealed that the overall noise of the imager was 28 e^- rms. This was much less than our nominal readout noise of 575–870 e^- rms. More importantly, the imager excess noise F was about unity. When the integration time (t_{int}) was halved, the noise almost doubled (at about 47 e^- rms), in agreement with the expected inverse scaling with integration time [21]. The integration capacitor of our off-the-shelf ROIC prevents longer t_{int}, and it is very difficult to make larger integration capacitors in small pixel sizes. However, it is possible to lower the dark current with better optimization of the manufacturing process, optimizing injector sizes or lowering the internal gain. After these optimizations, extrapolating the integration time suggests that an overall noise of less than 2 electrons rms at $t_{\mathrm{int}} = 10$ ms (100 frames/s) should be achievable.

Our nanoinjection imager utilizes an internal low-noise amplification mechanism to boost the SNR in a short-wave IR imager. We have demonstrated that the nanoinjection mechanism can provide 2 orders of magnitude improved SNR compared to a high-end short-wave IR imager and provide high sensitivity with low noise levels even at short integration times.

References

1. R. Sloan, J. H. Shaw, and D. Williams, J. Opt. Soc. Am. **46**, 543 (1956).
2. M. Vatsia, "Atmospheric optical environment, research and development," Tech. Rep. 7023 (ECOM, 1972).
3. E. Diamanti, C. Langrock, M. M. Fejer, Y. Yamamoto, and H. Takesue, Opt. Lett. **31**, 727 (2006).
4. D. S. Moore, Sens. Imaging **8**, 9 (2007).
5. R. H. Hadfield, Nat. Photon. **3**, 696 (2009).
6. E. Knill, R. Laflamme, and G. J. Milburn, Nature **409**, 46 (2001).
7. T. P. Spiller, Proc. IEEE **84**, 1719 (1996).
8. S. A. Castelletto, I. P. Degiovanni, V. Schettini, and A. L. Migdall, J. Mod. Opt. **54**, 337 (2007).
9. I. Hartl, X. D. Li, C. Chudoba, R. K. Ghanta, T. H. Ko, J. G. Fujimoto, J. K. Ranka, and R. S. Windeler, Opt. Lett. **26**, 608 (2001).
10. S. M. Sze, *Physics of Semiconductor Devices* (Wiley, 1981).
11. T. Martin, R. Brubaker, P. Dixon, M.-A. Gagliardi, and T. Sudol, Proc. SPIE **5783**, 12 (2005).
12. A. Joshi, J. Stevens, A. Kononenko, and J. Blackwell, Proc. SPIE **5499**, 228 (2004).
13. J. C. Campbell, S. Demiguel, M. Feng, A. Beck, G. Xiangyi, W. Shuling, Z. Xiaoguang, L. Xiaowei, J. D. Beck, M. A. Kinch, A. Huntington, L. A. Coldren, J. Decobert, and N. Tscherptner, IEEE J. Sel. Top. Quantum Electron. **10**, 777 (2004).
14. D. F. Murphy, M. Ray, R. Wyles, J. F. Asbrock, N. A. Lum, J. Wyles, C. Hewitt, A. Kennedy, D. Van Lue, J. S. Anderson, D. Bradley, R. Chin, and T. Kostrzewa, Proc. SPIE **4721**, 99 (2002).
15. M. A. Itzler, M. Entwistle, M. Owens, X. Jiang, K. Patel, K. Slomkowski, T. Koch, S. Rangwala, P. F. Zalud, Y. Yu, J. Tower, and J. Ferraro, Proc. SPIE **7320**, 73200O (2009).
16. O. G. Memis, A. Katsnelson, S. C. Kong, H. Mohseni, M. Yan, S. Zhang, T. Hossain, N. Jin, and I. Adesida, Appl. Phys. Lett. **91**, 171112 (2007).
17. O. G. Memis, A. Katsnelson, S. C. Kong, H. Mohseni, M. Yan, S. Zhang, T. Hossain, N. Jin, and I. Adesida, Opt. Express **16**, 12701 (2008).
18. J. B. Barton, R. F. Cannata, and S. M. Petronio, Proc. SPIE **4721**, 37 (2002).
19. M. M. Hayat, W. L. Sargeant, and B. E. A. Saleh, IEEE J. Quantum Electronics **28**, 1360 (1992).
20. S. D. Personick, *Fiber Optics: Technology and Applications* (Plenum, 1985).
21. B. E. A. Saleh, M. M. Hayat, and M. C. Teich, IEEE Trans. Electron Devices **37**, 1976 (1990).